Japanese Journal of Applied Physics **56**, 08MB03 (2017)
https://doi.org/10.7567/JJAP.56.08MB03

REGULAR PAPER

Bifacial aspects of industrial n-Pasha solar cells

Bas B. Van Aken*, Kees Tool, Eric J. Kossen, Anna J. Carr, Gaby J. M. Janssen, Bonna K. Newman, and Ingrid G. Romijn

ECN — Solar Energy, P.O. Box 1, 1755 ZG, Petten, The Netherlands

*E-mail: vanaken@ecn.nl

Received January 20, 2017; revised April 7, 2017; accepted April 10, 2017; published online June 30, 2017

Bifacial photovoltaic (PV) modules make optimal use of diffuse and ground-reflected light. The gain in energy yield depends on both the local climatic conditions and the PV system layout. These determine the additional irradiance on the rear of the PV panels. The rear response of the (laminated) solar cell(s) determines how much additional energy this rear irradiance generates. Based on our experiments and simulations, the main parameters that determine the bifaciality factor of solar cells with a front side junction are the rear metal coverage, the base resistivity and the diffusion profile on the rear. These will be evaluated and discussed in this paper. Front-junction solar cells with low base resistivity have a lower short circuit current when illuminated from the rear due to enhanced recombination in the BSF. Stencil printed rear metallization yields a higher bifaciality factor compared to screen printed by reducing the metal coverage and consumption and maintaining the front side efficiency. For our optimized 239 cm^2 bifacial cell we estimate that the output with 20% contributed by the rear side is equivalent to that of a 24.4% efficient monofacial cell.

1. Introduction

Bifacial solar cells with rear metal grid instead of a fully metallized rear are already commercialized. Bifacial cells produced by Yingli,[1)] Mission Solar, LG, and PVGS[2)] are of the passivated emitter, rear totally diffused type (PERT).[3–6)] The bifacial cells produced by Panasonic/Sanyo are based on heterojunction technology.[7)] Other cell types such as variations of the passivated emitter and rear cell (PERC)[8,9)] and even back contact cell concepts can be bifacial.[10–13)] When bifacial cells are mounted in a module with a reflecting back sheet or with a reflecting material between the cells, a high monofacial module efficiency is obtained.[14)] But with a transparent rear, glass–transparent back sheet layout[15)] or, glass–glass[15–17)] reflected and diffuse light as well as direct light falling on the rear can add 20% or more to the energy output depending on the location, albedo and orientation of the module.[18–20)] As additional costs are small, application of bifacial modules has the potential of a significant reduction of the levelised cost of electricity.

The photovoltaic (PV) system layout and the local irradiance conditions determine the amount of, mostly, diffuse and ground-reflected light on the rear of bifacial modules.[21–23)] The rear response of the (laminated) solar cell(s) determines how much additional energy this rear irradiance generates. Based on experiments and simulations, some of the main parameters that determine the bifaciality factor of solar cells, including base resistivity, metal coverage and the back-surface field (BSF), will be discussed.

2. Experimental methods

The n-Pasha solar cells (Czochralski-silicon, Cz-Si, M0 wafers, 239 cm^2) are manufactured with standard processes on industrial tools as reported before.[24,25)] Random pyramid texture is obtained with alkaline wafer etching. The diffused emitter and BSF are processed using industrial tube furnaces by Tempress.[26)] The emitter is made using BBr_3 as precursor, the BSF is made using $POCl_3$ as precursor. The additional lateral conductivity in the phosphorus doped BSF contributes to a good fill factor (FF) despite the open rear side metallization and increases the tolerance to high substrate resistivities. SiN_x layers for passivation and anti-reflective (AR) coating are deposited on the front and on the rear side. Screen or stencil printing[27–29)] can be used to apply the front and rear side metallization grids. Both metallization grids are fired in a single step in an IR-heated belt furnace. The current–voltage (I–V) measurements have been conducted with a Class AAA solar simulator (Wacom) on a non-conductive, low reflective (anodized) chuck according to the IEC standard.[30)]

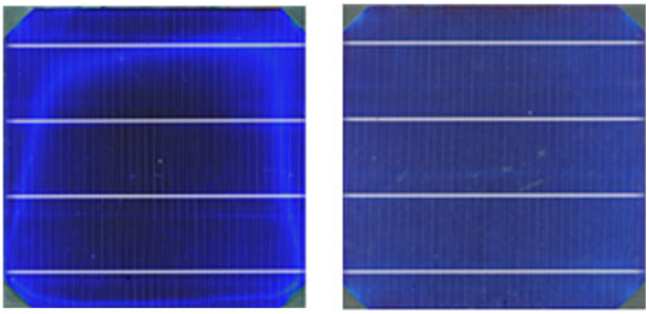

Fig. 1. (Color online) Photographs of rear side of n-Pasha solar cells with (left) standard uniform BSF and (right) optimized uniform BSF, by improved co-diffusion.

3. Results

For application in monofacial solar panels, the optical properties of the BSF are not the most important factor. Typically, the BSF is only optimized for passivation and conduction properties. However, for bifacial application, the optical behavior becomes more important. Figure 1 shows the appearance of the rear side of n-Pasha solar cells with uniform BSF (u-BSF) before and after optimization of the homogeneity of the u-BSF. The solar cells with the more homogeneous u-BSF show an improved rear side efficiency.

However, a higher front-side efficiency can be achieved by a selective BSF (s-BSF). Solar cells with a s-BSF have been manufactured by etch-back on wafers with resistivities in the range 1.5 to 9 Ω cm. Compared to the standard s-BSF solar cells, the optimized s-BSF cells have a larger area that is etched back. The short circuit current density J_{sc} and the

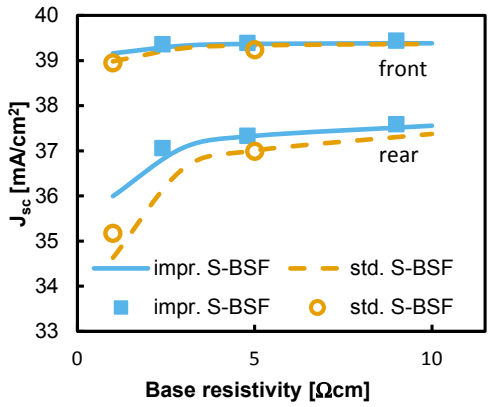

Fig. 2. (Color online) Front and rear short circuit density as a function of base resistivity. Symbols represent experimental data for standard BSF (closed blue) and optimized BSF (red, open). Solid red and dashed blue lines indicate the modelling results, respectively for standard and optimized BSF.

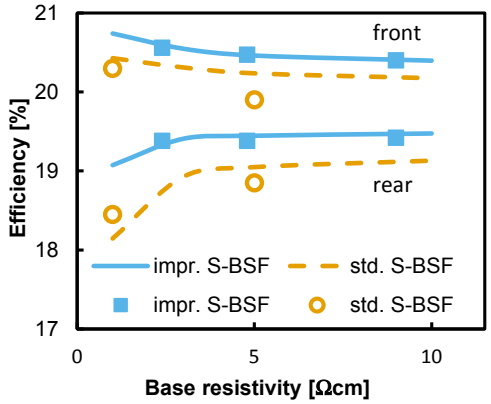

Fig. 3. (Color online) Front and rear efficiency as a function of base resistivity. Symbols represent experimental data for standard BSF (closed blue) and optimized BSF (red, open). Solid blue and dashed red lines indicate the modelling results, respectively for optimized and standard BSF.

efficiency η are plotted in Figs. 2 and 3, respectively. Increasing the etched-back area of the s-BSF has a positive influence on both the front and the rear efficiency as can be seen in Fig. 3. For a base resistivity of 5 Ω cm, the front efficiency improves by 0.2% absolute, the rear efficiency by 0.4%. This corresponds to a 2% relative increase in bifaciality factor, i.e., the rear efficiency normalized to the front efficiency. Figures 2 and 3 also shows that for low base resistivity the difference between illuminating the front and rear side of the solar cells increases strongly. In other words, the bifacial factor becomes smaller at low base resistivity.

We have also simulated these solar cells under front and rear illumination. The simulations were done with a parameterization similar to the n-Pasha parameterization described elsewhere, resulting in an efficiency of about 20.7%.[31] We extracted the front and rear J_{sc} and front and rear η as function of the base resistivity, the data is plotted as lines in Figs. 2 and 3. The front and rear J_{sc} are in good quantitative agreement with the measured data. Although the same qualitative behavior is seen for the simulated and measured efficiencies, the match is not so good due to differences in simulated and observed fill factors. The differences are caused by experimental group-to-group variations of the external resistances, whilst the simulation

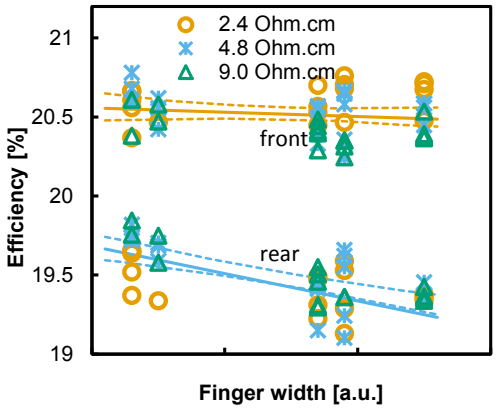

Fig. 4. (Color online) Front and rear efficiency as a function of rear side finger width for three wafer resistivities, as indicated in the legend. Symbols represent experimental data, the lines indicate the average efficiency, independent of base resistivity, with the dashed lines indicating the 95% confidence intervals.

parameter for the external resistivity was kept constant. Also pseudo FF effects, e.g., due to inhomogeneities, are not corrected for. The relation between the ratio of front and rear J_{sc} and the recombination properties of the two BSF processes will be explained in the discussion.

In contrast, the V_{oc} is hardly dependent on the base resistivity and the illumination side. In our simulations, assuming a bulk lifetime of 1 ms, only a small increase, <1 mV, in V_{oc} was observed below 3 Ω cm compared with high base resistivity for front side illumination (not shown).

The FF is lowest for material with a base resistivity of 10 Ω cm. With decreasing base resistivity, the FF significantly increases with 2 to 3% relative, especially for base resistivities below 3 Ω cm, both for front and rear illumination (also not shown). The combined effects on J_{sc}, FF, and V_{oc} are that the front side efficiency slightly improves with decreasing base resistivity whereas the rear side efficiency decreases, dominated by effects on the J_{sc}. At 1 Ω cm, the difference in simulated total gain is 1.5% absolute (see Fig. 3).

The final parameter that controls the bifaciality is the metallization. The design of the rear side metal grid is a competition between Ag consumption, area coverage and resistive losses. Bifacial solar cells were manufactured on wafers with base resistivity of 2.4, 4.8, and 9.0 Ω cm. The rear metal coverage was varied by changing the number and width of the fingers on the screen design and also the printing process parameters. In Fig. 4, the front and rear efficiency is plotted as a function of the finger width. Clearly, for front side illumination, there is no dependence of the efficiency on the rear finger width. The front efficiency seems also not to have a significant dependency on the base resistivity.

In contrast, the rear side efficiency does increase with decreasing rear finger width. The lower shading by the smaller finger width leads to a higher rear J_{sc}. For low resistive wafers, the rear efficiency increase at the smallest finger widths is less pronounced as the bifaciality is lower (see Fig. 3).

Figure 5 shows the FF and the efficiency of the cells for front side illumination as a function of the rear Ag paste consumption for the different base resistivities. The effect of the base resistivity (different colors in Fig. 5) on the front

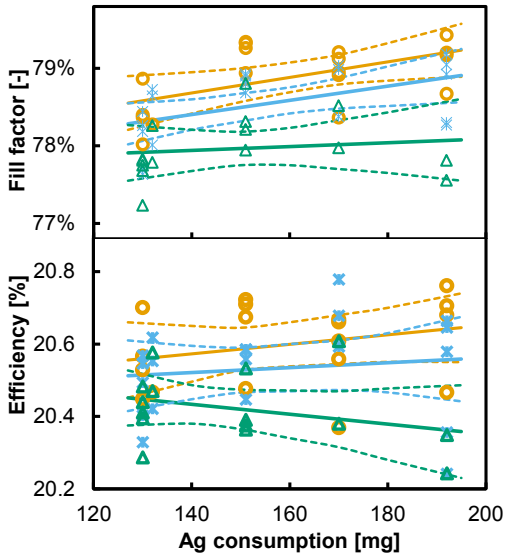

Fig. 5. (Color online) Front fill factor and efficiency as a function of rear side Ag consumption for three wafer resistivities, as indicated in the legend of Fig. 4. Symbols represent experimental data, solid and dashed lines indicate the average efficiency and 95% confidence intervals.

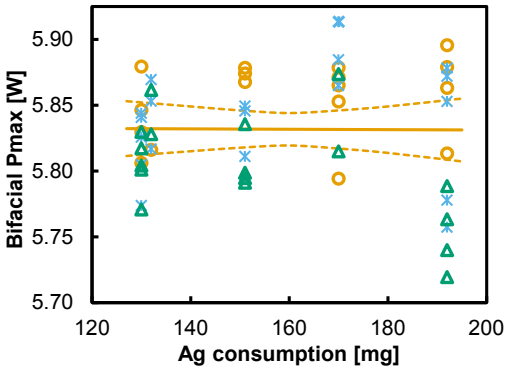

Fig. 6. (Color online) Bifacial power output as a function of rear side Ag consumption for three wafer resistivities, as indicated in the legend of Fig. 4. Symbols represent experimental data, solid and dashed lines indicate the average efficiency and 95% confidence intervals. The bifacial power output is calculated for 1 sun irradiance at the front and 0.2 sun irradiance at the rear.

side FF and front efficiency is more pronounced than the effect of the rear Ag consumption (horizontal axis), at least within the experimental ranges of this experiment. The trend lines of the front side FF for solar cells on wafers with 2.4 and 4.8 Ω cm show a small, hardly significant, decrease with decreasing Ag consumption as the resistive losses increase at lower Ag consumption. The solar cells on 9.0 Ω cm wafers do not show this increase in resistive losses, as the lateral conductivity in the wafer is limiting the front side FF. Note that the *I*–*V* curves were measured using a non-conductive chuck.

The FF decrease with decreasing rear Ag consumption is compensated by the positive trend in J_{sc} and V_{oc}. A lower Ag contact area contributes to a decrease in the contact recombination losses, in turn improving the J_{sc} and V_{oc}. The resulting front efficiency does not change significantly with decreasing rear Ag consumption. An average value of 20.5% is found, for the three wafer resistivities, at a rear Ag consumption of only 130 mg. This value is in the same range as the amount printed on the front side. As there is no indication of a decrease in front efficiency with decreasing Ag consumption, the optimum can be at even lower Ag consumption without front side efficiency losses.

As the base resistivity has opposite effects on the efficiency for front and rear illumination, we have calculated a weighted bifacial efficiency, assuming a 1000 W/m^2 irradiation from the front and 200 W/m^2 from the rear. In a first approximation the bifacial efficiency η_{bif} is then calculated from the front and rear efficiency as

$$\eta_{bif} = \eta_{front} + 0.2\eta_{rear}. \quad (1)$$

Note that this definition does not account for the counteracting effects of increased V_{oc} and for the higher resistive losses that result from the higher total current. The resulting bifacial power output is plotted in Fig. 6. No trend is observed in the data, suggesting that within the range of solar cells that were manufactured in this study, no dependency of the bifacial power output on the base resistivity nor on the Ag consumption can be resolved. The average bifacial power of 5.83 W for a 239 cm^2 solar cell is equivalent to a 24.4% monofacial solar cell at 1000 W/m^2 front side illumination.

4. Discussion

To understand the influence of the base resistivity of the wafer on the bifaciality factor, first the implications of front or rear irradiance on the charge carrier generation and the recombination current is explained. Comparing front illumination with rear illumination for front-junction solar cells, the main effect is that with rear illumination the minority charge carriers have to travel through the bulk towards the junction when a current is drawn from the cell. This increases the excess concentration, Δn, near the illuminated side, the BSF. The recombination current at the BSF is proportional to both the donor concentration and the excess concentration. A higher donor or a higher excess concentration will therefore reduce the J_{sc} because they increase the recombination current. This means that the recombination losses are larger for rear illumination because Δn is larger. It also implies that, as with decreasing base resistivity the donor concentration increases, the J_{sc} for front and for rear illumination decreases with decreasing base resistivity.

The results of Fig. 2 can be fully explained by this description. First, for a given BSF process, an increase in the rear J_{sc} is observed with increasing base resistivity, i.e., decreasing donor concentration. At lower donor concentration, the description above stipulates that the BSF recombination current decreases and thus the rear J_{sc} increases, in line with the experimental observations. Second, the improved BSF process reduces the recombination properties of the BSF. This process also reduces the BSF recombination current. Therefore the rear J_{sc} of the standard BSF decreases faster with decreasing base resistivity than the rear J_{sc} of the improved BSF (see base resistivity Fig. 2).

Whereas at short-circuit conditions the transport of current determines the distribution of the excess concentration, at open circuit conditions the distribution of the excess concentration results from the recombination properties of the cell. The recombination properties are not sensitive to the illumination side. Therefore the V_{oc} is in first order not affected by the illumination side, in contrast with the J_{sc}. Moreover, the V_{oc} is hardly dependent on the base resistivity,

as at open circuit conditions n-Pasha solar cells are in high level injection conditions. This means that the majority concentration is determined by the excess concentration rather than the doping concentration.

Figure 4 shows that with decreasing rear finger width, there is no change in the front efficiency. In contrast, a steady increase in rear efficiency is observed, except for the most narrow fingers on wafers with the lowest resistivity. The front efficiency for this range of finger widths is in balance between the FF, which decreases with decreasing finger width, and the J_{sc} and V_{oc}, which increase with decreasing contact area, and thus with finger width. In contrast, for the rear efficiency the original process that applied the highest finger width in Fig. 4, is clearly not near the optimum. Decreasing the finger width not only reduces the contact area and associated contact recombination losses, but also decreases the shaded fraction of the wafer surface, thus increasing J_{sc}.

The efficiency bin distribution is partly influenced by variation in base resistivity of the wafers, which is typically larger in n-type compared to p-type. For different base resistivities, the trend lines of FF and front efficiency converge at lower Ag consumption (Fig. 5). Due to this convergence, the efficiency is less depended on base resistivity at lower Ag consumption. Besides reducing the Ag consumption, this observed convergence reduces the efficiency bin distribution of n-PERT solar cells.

5. Conclusions

We have shown that the bifaciality factor of front junction cells depends on the base resistivity, the BSF properties and the metal coverage. Simulation results support the experimental observation that the bifaciality factor is higher for higher base resistivity. Within the present study, reduction of the rear metal coverage, i.e., narrower fingers and lower Ag consumption, increases the bifaciality without compromising the front side efficiency. Although the lower Ag consumption decreases the front side FF, its effects are compensated by the increasing trend in front side J_{sc} and V_{oc}. An average efficiency of 20.5% is obtained at a Ag consumption of only 130 mg at the rear side. The bifacial power output is equivalent to a 24.4% monofacial solar cell.

Acknowledgements

This work was partially funded by the Dutch TKI Solar Energy projects Antilope and Champ and TKI-toeslag project BING (http://www.tki-urbanenergy.nl/).

1) A. R. Burgers, R. C. G. Naber, A. J. Carr, P. C. Barton, L. J. Geerligs, X. Xiong, L. Li, S. Weipeng, A. Haijiao, H. Hu, P. R. Venema, and A. H. G. Vlooswijk, Proc. 25th European Photovoltaic Solar Energy Conf. Exhib. (EU PVSEC), 2010, p. 1106.
2) S. Gonsui, S. Goda, K. Sugibuchi, N. Ishikawa, K. Honda, and H. Zama, Proc. 28th European Photovoltaic Solar Energy Conf. Exhib. (EU PVSEC), 2013, p. 718.
3) V. D. Mihailetchi, J. Jourdan, A. Edler, R. Kopecek, R. Harney, D. Stichtenoth, J. Lossen, T. Böscke, and H.-J. Krokoszinski, Proc. 25th European Photovoltaic Solar Energy Conf. Exhib. (EU PVSEC), 2010, p. 1446.
4) D. Kania, T. S. Böscke, M. Braun, P. Sadler, C. Schöllhorn, M. Dupke, D. Stichtenoth, A. Helbig, R. Carl, K. Meyer, A. Grohe, J. Lossen, and H.-J. Krokoszinski, 28th European Photovoltaic Solar Energy Conf. Exhib. (EU PVSEC), 2013, p. 1383.
5) R. Cabal, T. Blévin, R. Monna, Y. Veschetti, and S. Dubois, Energy Procedia **92**, 684 (2016).
6) F. Kiefer, J. Krügener, F. Heinemeyer, M. Jestremski, J. Osten, R. Brendel, and R. Peibst, Sol. Energy Mater. Sol. Cells **157**, 326 (2016).
7) M. Taguchi, A. Yano, S. Tohoda, K. Matsuyama, Y. Nakamura, T. Nishiwaki, K. Fujita, and E. Maruyama, IEEE J. Photovoltaics **4**, 96 (2014).
8) T. Dullweber, C. Kranz, R. Peibst, U. Baumann, H. Hannebauer, A. Fülle, S. Steckemetz, T. Weber, M. Kutzer, M. Müller, G. Fischer, P. Palinginis, and H. Neuhaus, Proc. 31st European Photovoltaic Solar Energy Conf. Exhib. (EU PVSEC), 2015, p. 341.
9) T. Dullweber, C. Kranz, R. Peibst, U. Baumann, H. Hannebauer, A. Fülle, S. Steckemetz, T. Weber, M. Kutzer, M. Müller, G. Fischer, P. Palinginis, and H. Neuhaus, Prog. Photovoltaics **24**, 1487 (2016).
10) C. Z. Zhou, P. Y. Verlinden, R. A. Crane, R. M. Swanson, and R. A. Sinton, Proc. 26th IEEE Photovoltaic Specialists Conf. (PVSC), 1997, p. 287.
11) S. W. Glunz, J. Knobloch, C. Hebling, and W. Wettling, Proc. 26th IEEE Photovoltaic Specialists Conf. (PVSC), 1997, p. 231.
12) I. Cesar, N. Guillevin, A. R. Burgers, A. A. Mewe, M. Koppes, J. Anker, L. J. Geerligs, and A. W. Weeber, Energy Procedia **55**, 633 (2014).
13) V. D. Mihailetchi, H. Chu, G. Galbiati, C. Comparroto, A. Halmand, and R. Kopecek, Energy Procedia **77**, 534 (2015).
14) B. B. Van Aken, L. A. G. Okel, J. Liu, S. L. Luxembourg, and J. A. M. Van Roosmalen, Proc. 32nd European Photovoltaic Solar Energy Conf. Exhib. (EU PVSEC), 2016, p. 42.
15) J. P. Singh, S. Guo, I. M. Peters, A. G. Aberle, and T. M. Walsh, IEEE J. Photovoltaics **5**, 783 (2015).
16) E. Saint-Sernin, R. Einhaus, K. Bamberg, and P. Panno, Proc. 23rd European Photovoltaic Solar Energy Conf. Exhib. (EU PVSEC), 2008, p. 2825.
17) B. Liu, Y. Chen, Y. Yang, J. Dong, H. Shen, Z. Feng, and P. Verlinden, Proc. 31st European Photovoltaic Solar Energy Conf. Exhib. (EU PVSEC), 2015, p. 659.
18) K. Sugibuchi, N. Ishikawa, and S. Obara, Proc. 28th European Photovoltaic Solar Energy Conf. Exhib. (EU PVSEC), 2013, p. 4312.
19) A. Lindsay, M. Chiodetti, D. Binesti, S. Mousel, E. Lutun, K. Radouane, and J. Christopherson, Proc. 32nd European Photovoltaic Solar Energy Conf. Exhib. (EU PVSEC), 2016, p. 1610.
20) A. Cuevas, A. Luque, J. Eguren, and J. del Alamo, Sol. Energy **29**, 419 (1982).
21) J. A. Duffie and W. A. Beckman, *Solar Engineering of Thermal Processes* (Wiley, New York, 1991) 2nd ed., Chap. 2.
22) U. A. Yusufoglu, T. H. Lee, T. M. Pletzer, A. Halm, L. J. Koduvelikulathu, C. Comparotto, R. Kopecek, and H. Kurz, Energy Procedia **55**, 389 (2014).
23) A. Lindsay, M. Chiodetti, P. Dupeyrat, D. Binesti, E. Lutun, and K. Radouane, Proc. 31st European Photovoltaic Solar Energy Conf. Exhib. (EU PVSEC), 2015, p. 1764.
24) I. G. Romijn, B. B. Van Aken, J. Anker, A. R. Burgers, A. Gutjahr, B. Heurtault, M. Koppes, E. Kossen, M. Lamers, D. S. Saynova, C. J. J. Tool, L. Fang, J. Xiong, G. Li, X. Zhuo, H. Wang, Z. Hu, P. R. Venema, and A. H. G. Vlooswijk, Proc. 27th European Photovoltaic Solar Energy Conf. Exhib. (EU PVSEC), 2012, p. 533.
25) M. K. Stodolny, G. J. M. Janssen, B. B. Van Aken, C. J. J. Tool, M. W. P. E. Lamers, I. G. Romijn, P. R. Venema, M. R. Renes, O. Siarheyeva, E. H. A. Granneman, J. Wang, J. Ma, J. Cui, F. Lang, Z. Hu, and J. Löffler, Proc. 32nd European Photovoltaic Solar Energy Conf. Exhib. (EU PVSEC), 2016, p. 1908.
26) Y. Komatsu, V. D. Mihailetchi, L. J. Geerligs, B. van Dijk, J. B. Rem, and M. Harris, Sol. Energy Mater. Sol. Cells **93**, 750 (2009).
27) G. Yao, Ph.D. thesis, University of New South Wales (2005).
28) J. Hoornstra and B. Heurtault, Proc. 24th European Photovoltaic Solar Energy Conf. Exhib. (EU PVSEC), 2009, p. 989.
29) H. Hannebauer, T. Falcon, J. Cunnusamy, and T. Dullweber, Energy Procedia **98**, 40 (2016).
30) IEC 60904-1 (2006).
31) A. Fell, K. R. McIntosh, P. P. Altermatt, G. J. M. Janssen, R. Stangl, A. Ho-Baillie, H. Steinkemper, J. Greulich, M. Muller, B. Min, K. C. Fong, M. Hermle, I. G. Romijn, and M. D. Abbott, IEEE J. Photovoltaics **5**, 1250 (2015).

